Mineralogia, vol. 56, 2025, 4-12 *Original Paper*

DOI: 10.2478/mipo-2025-0002

Syn-volcanic melt-rock reactions recorded in peridotitic xenoliths from Scania, S Sweden

Anna Kukuła[1,*], Magdalena Matusiak-Małek[2], Jakub Mikrut[2], Theodoros Ntaflos[3], Leif Johansson[4]

[1]Institute of Geological Sciences, Polish Academy of Sciences, Podwale 75, 50-449 Wrocław, Poland
[2]Institute of Geological Sciences, University of Wrocław, Pl. M. Borna 9, 50-204 Wrocław, Poland
[3]Department of Lithospheric Research, University of Vienna, Althanstrasse 14, 1090 Vienna, Austria
[4]Department of Geology, Lund University, Sölvegatan 12, 223 62 Lund, Sweden

*Corresponding author:
a.kukula@twarda.pan.pl

Abstract

Peridotite xenoliths from Scania (S Sweden), brought to the surface by Mesozoic basanitic magmas, provide insights into the lithospheric mantle underlying the East European Craton. During their ascent, some of the entrained xenoliths were infiltrated by a Si-undersaturated melt. The infiltration triggered orthopyroxene dissolution and the formation of fine-grained olivine, clinopyroxene and Si-rich glasses (trachytic/trachydacitic and dacitic). The latter interacted with clinopyroxene and/or spinel creating spongy rims of various thicknesses (from few to hundreds of µm). The reactions varied in intensity and effect depending on the distance from the xenolith margin and the duration of the reaction time. At the outer parts of xenoliths, intense reactions dissolved orthopyroxene entirely, forming spongy rims on spinel and clinopyroxene, while inner sections showed limited reactions, primarily between mafic melts and orthopyroxene. The local reheating and melting of fine-grained aggregates during the ascent of xenoliths resulted in the formation of a hydrous, high-Mg, glass-like phase.

Keywords: upper mantle xenoliths, melt infiltration, orthopyroxene breakdown, fine-grained aggregates, spongy domains

1. Introduction

The mineral and chemical composition of the lithospheric mantle is the result of various processes, including metasomatism and melting events. A rapid ascent (~ 6 m/s; Demouchy et al., 2006) of peridotitic xenoliths in basaltic magmas to the Earth's surface minimizes the extent of their alteration and allows the preservation of relatively clear records of mantle processes. Conversely, the host magma can chemically interact with the xenoliths, altering both their texture and chemical composition. These processes can obscure the primary signatures of mantle processes, making them challenging to interpret (Shaw & Dingwell, 2008; Shaw, 2009; Marchev et al., 2017).

Peridotitic xenoliths from Scania (S Sweden; Erlström, 2009) were carried to the surface by Mesozoic mafic alkaline lavas and sampled the lithospheric mantle underneath the south-west margin of the East European Craton (Artemieva, 2003). The mineral chemical composition of the peridotites is strongly variable (Rehfeld et al., 2007), indicating a heterogeneous source region affected by carbonatitic and (possibly) alkaline-silicate metasomatisms (Mikrut et al., 2019). In some xenoliths, the rock-forming minerals are accompanied by fine-grained aggregates, whereas clinopyroxene and spinel are locally surrounded by spongy rims. Various models have been proposed in the literature to explain the formation of these structures, such as interaction with host magma during entrainment (Shaw & Klügel, 2002; Shaw et al., 2006), interaction with a metasomatic agent before ascent (Ionov et al., 1994; Coltorti et al. 1999), or fluid-inducted incongruent decompression melting event occurring under mantle

conditions (Carpenter et al., 2002), decompression-induced partial melting (Su et al. 2011; Pan et al. 2018) or sub-solidus reaction during decompression of a garnet peridotite (Falus et al., 2000). Such mechanisms involve mantle reactions and may represent a significant stage in mantle evolution. Consequently, it is essential to determine whether the fine-grained structures are intrinsic to mantle evolution or formed later, during the uplift of the xenoliths. This study aims to identify the relative timing of the formation of these structures in the mantle xenoliths from Scania.

2. Geological context

Scania region (S Sweden) is located at the south-west margin of the East-European Craton (Fig. 1). The predominant lithologies are 1.71 - 1.66 Ga old granitoids and orthogneisses of Trans-Scandinavian Igneous Belt (Johansson et al., 2006). Some of these rocks, located west of the Sveconorvegian Front (Fig. 1), were later deformed during the Sveconorwegian orogeny (1.2 – 0.9 Ga; Bingen et al., 2021).

In the Mesozoic (Jurassic or Jurassic-Cretaceous) this area was affected by volcanic activity (Bergelin et al., 2011; Tappe et al., 2016) associated with the rifting of the south-west periphery of the East-European Craton (Tappe, 2004). This volcanic episode produced mafic alkaline melts, mostly basanites and melanefelinites (Tappe, 2004). Xenoliths of felsic, mafic, and ultramafic rocks carried by the volcanics sample the upper mantle and various levels of the crust beneath Scania (Rehfeldt et al., 2007).

Ultramafic xenoliths from Scania are usually 4 to 10 cm in diameter. The contact of host basanite with olivine from xenoliths is sharp, while that with clinopyroxene is underlined by stocked subhedral clinopyroxene crystals (100–300 µm long; Fig. 2A). The behavior of orthopyroxene at the contact with basanite remains unclear, due to its scare presence in this position. Textures of the peridotites vary from equigranular (SA28, Fig. 2B), protogranular to porphyroclastic with numerous subtypes. They are spinel lherzolites and harzburgites, scarcely dunites (Mikrut et al., 2019). The chemical composition of the rock-forming minerals of Scania peridotites is heterogeneous, both within the sample set and within specific samples. Peridotite-forming olivine has forsterite (Fo=Mg/(Mg+Fe^{tot})x100) content between 89.5 and 91.7. The Mg# (Mg/(Mg+Fe^{tot})) of orthopyroxene is 89.7 – 92.0 and that of clinopyroxene is 89.6 – 93.4, while Cr# (Cr/(Cr+Al)) of spinel is 0.21 – 0.37 (Mikrut et al., unpublished data; Rehfeld et al., 2007). Scania peridotites with high Fo-olivine (91.2-91.7) were interpreted as mantle peridotites strongly affected by mafic melts, while those with Fo=89.5-91.1 represent peridotites metasomatized by carbonatites (Mikrut et al., 2019).

In this study, we examine the origin of intergranular fine-grained aggregates in ultramafic xenoliths from two basanites localities: Säte (averaged age is 167 Ma; Bergelin et al., 2011) and Skuddarp (Fig. 1). Spinel lherzolites from those localities were interpreted by Rehfeld et al. (2007) as mantle rocks depleted in 8-13 % and possibly affected by hydrous metasomatic melts.

3. Analytical methods

The results presented in this research are based on detailed petrographic studies of 18 xenoliths but the fine-grained structures being the topic of this study occur only in 8 xenoliths (S16E, S23, SA24, SA28, SK120, SK121, SK122, SK124). The back-scattered images were made using a scanning electron microscope JEOL JSM IT100 In-Touch-Scope™ equipped with an Oxford X-Act energy dispersive spectrometer (SEM-EDS), working at an accelerating voltage of 15 kV and probe current 60 nA in the Institute of Geological Sciences, University of Wroclaw, Poland.

The chemical compositions of minerals were determined using the Electron Probe Microanalyzer (EPMA) Cameca SXFive FE at the Department of Lithospheric Research, University of Vienna, Austria. The analytical conditions were: acceleration voltage 15 kV, beam current 20 nA. Natural silicates and synthetic oxides served as standards. The composition of glass in sample SA28 was determined with Jeol Superprobe electron microprobe with acceleration voltage 15 kV, beam current 40 nA at the Faculty of Geology, Geophysics and Environment Protection, AGH University of Krakow, Poland.

4. Textural features of the intergranular structures

According to the classification by Matusiak-Małek et al. (2014), three textural types of minerals are recognized: type I – coarse-grained primary minerals (olivine, clinopyroxene, orthopyroxene, spinel); type II (not discussed in this article) - exsolution lamellae in type I; and type III – intergranular aggregates (including spongy rims) consisting of fine grains of olivine, clinopyroxene, glass, and spinel.

We have defined two dominating intergranular structures in Scania xenoliths: fine-grained aggregates (1-5 mm in diameter) composed of clinopyroxene III, olivine III, ±glass (Fig. 2C-E) and spongy rims (few to several hundreds of µm thick) surrounding clinopyroxene I and spinel I (Fig. 2F,G). In the proximity of the aggregates, an altered, hydrous high-Mg glass-like phase (described as "OH-phase" by Rehfeld et al., 2007) is commonly found (Fig. 2C-E).

4.1. Textural features of fine-grained aggregates

The fine-grained aggregates usually develop at the margin of orthopyroxene I grains (Fig. 2C,D). The distribution of the minerals and melt in the aggregates are not homogeneous and the modal composition varies according to its thickness: the narrowest (20-30 µm wide) are formed of single, vermicular crystals of clinopyroxene III, glass and minute olivine III, often with enclosed oval grains of orthopyroxene (Fig. 2C); in

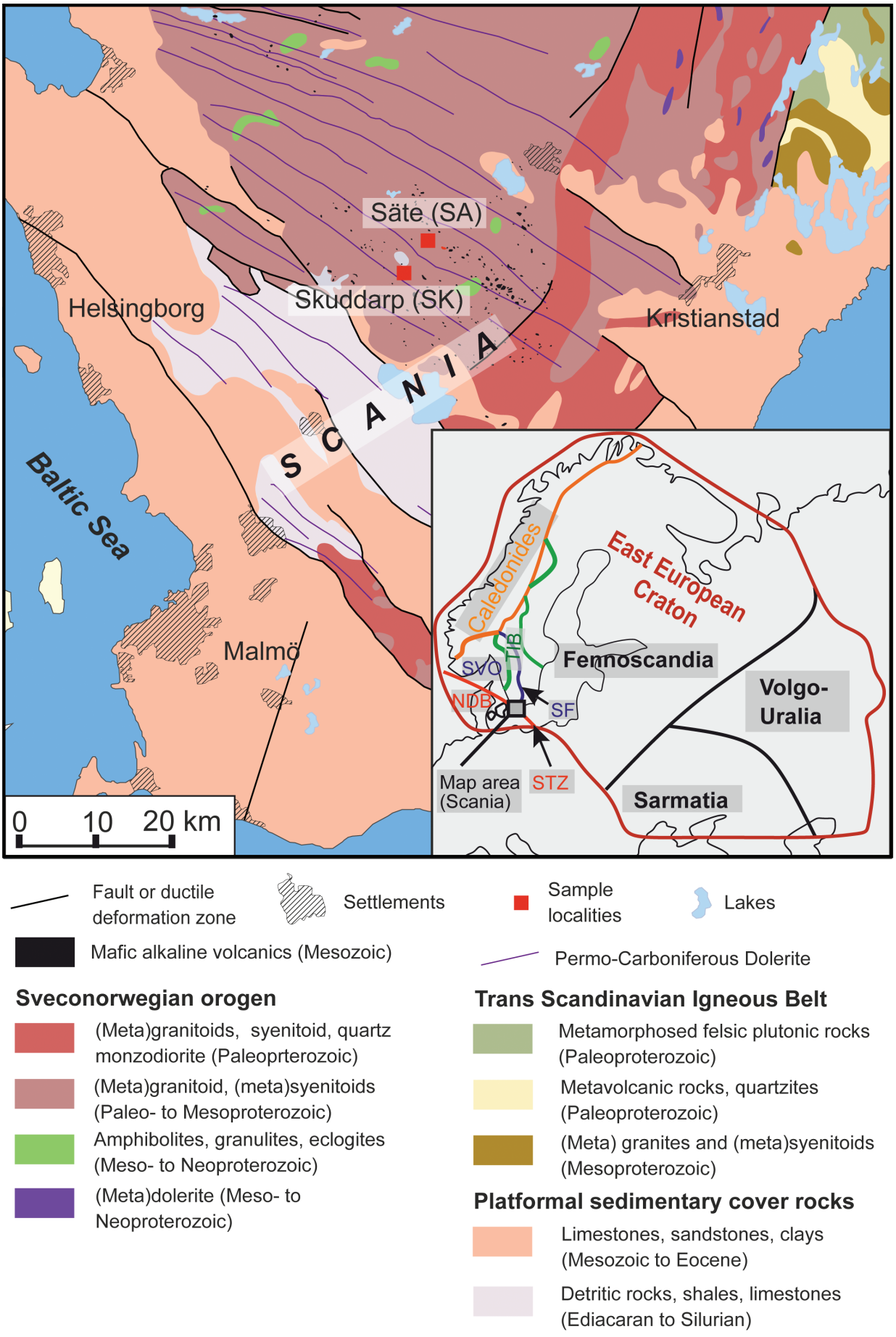

Figure 1. Localities of Mesozoic mafic alkaline volcanics in the Scania region, red squares mark vents from which the studied xenoliths were collected. Säte (SA), Skuddarp (SK). Inset shows schematic geotectonic position of Scania, STZ – Sorgenfrei-Tornquist Zone, SVO – Sveconorwegian Orogen, SF – Sveconorwegian Front, TIB – Trans Scandinavian Igneous Belt, NDB – Norwegian-Danish basin. Compiled from Asch (2005), Babuška & Plomerová (2004), Bingen et al. (2021) and Geological Survey of Sweden Digital Database (2018).

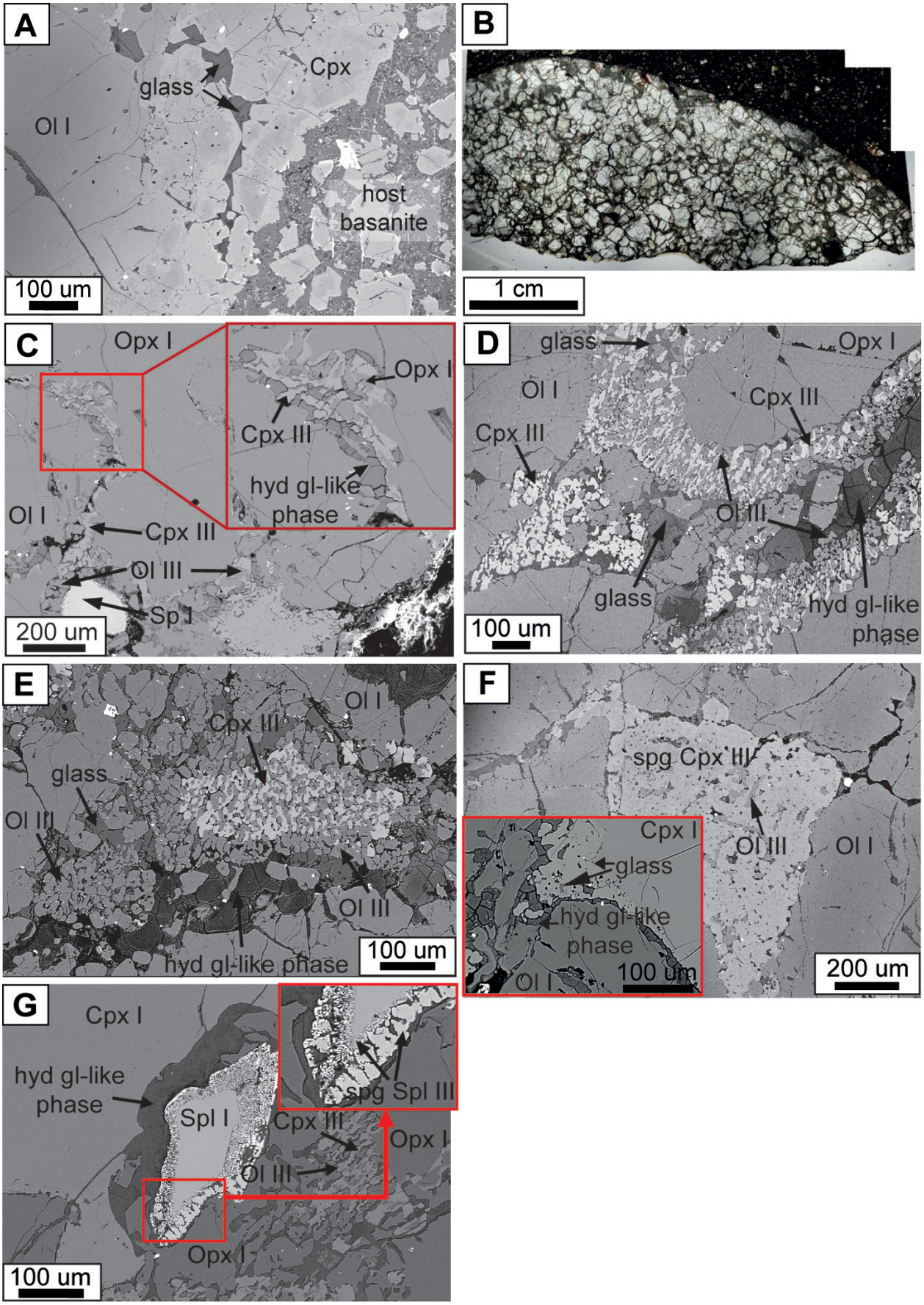

Figure 2. Microtextural features related to presence of aggregates in peridotitic xenoliths from Scania: (A) Contact between the host basanite and xenolith SA28 ("back-scattered electron image" – BSE image); (B) Equigranular texture in sample SA28 (plane polarized light); (C) Thin aggregates occurring between grains of orthopyroxene I and olivine I, inset shows enlargement of the area indicated by rectangle (sample SA28; BSE image); (D) Thick aggregates formed of parallel crystals of clinopyroxene III and olivine III and glass enveloping orthopyroxene I and spongy clinopyroxene (lower left corner; sample SA28; BSE image); (E) Aggregates formed of clinopyroxene III, olivine III, and glass, note the absence of orthopyroxene I in the core (sample SA28; BSE image); (F) Spongy clinopyroxene enclosing grains of olivine III (BSE images); inset shows the spongy margin of clinopyroxene with minute pools of glass and surrounded by vein of altered, hydrous high Mg glass-like phase (sample SA28); (G) Spinel I grain surrounded by spongy rims (BSE images); inset show dual structure of spinel spongy rim (sample SK121); hyd gl-like phase stands for altered, hydrous, high Mg glass-like phase; spg stands for spongy.

thicker aggregates (exceeding ~50 μm) clinopyroxene III becomes elongated, perpendicular to the contact with orthopyroxene I, grains of olivine III are oval and glass is present in interstices (Fig. 2D). In the biggest aggregates, orthopyroxene I is lacking (Fig. 2E) and the outermost part of the aggregate is formed of euhedral, olivine III grains (10-50 μm; Fig. 2E), whereas the innermost part is usually formed of radially-arranged grains of clinopyroxene III and olivine III (20–100 μm long); glass is present in interstices in both zones of the aggregates. Moreover, oval, fine (5-20 μm) grains of olivine locally form aggregates up to 100 μm in size embedded in glass (Fig. 2E). In areas closer to the margin of xenolith all the fine-grained structures were noticed, while in the inner parts, only the narrowest type is present.

The altered, hydrous, high-Mg glass-like phase surrounds fine-grained aggregates. It forms pools or veins of varying widths, which are less abundant in areas associated with the narrow aggregates (Fig. 2C). Conversely, in the presence of thicker fine-grained aggregates or between two fine-grained zones, this phase becomes more abundant (Fig. 2D,E).

4.2. Textural features of spongy domains

The spongy textures are consistently in contact with glass or with the altered, hydrous, high-Mg glass-like phase. The thickness of spongy clinopyroxene III rims surrounding clinopyroxene I varies from few to hundreds of μm. Small glass droplets within these spongy rims are from 1 to 5 μm. Clinopyroxene grains exhibiting a fully spongy texture are also present (Fig. 2F). The spongy spinel III rims surrounding spinel I consist either of a 20-100 μm-wide zone of vermicular (2-5 μm thick) spinel III crystals or are formed of a loose network of acicular crystals perpendicular to the margin of spinel I (Fig. 2G).

5. Chemical composition of phases forming intergranular structures

5.1. Chemical composition of phases forming fine-grained aggregates and altered, hydrous, high-Mg glass-like phase

The composition of type III phases forming fine-grained aggregates varies between samples and thus must be discussed in comparison with the composition of rock-forming minerals from the same sample (Fig. 3).

Clinopyroxene III forming aggregates has Mg#=89.2-93.4 (Fig. 3A; Table S1) and the Al and Na contents are 0.023-0.216 and 0.029-0.059 apfu, respectively (Fig. 3A,B; Table S1). Within a single sample, the Mg# increases, while the Al and Na decrease with the development of the thickness of the aggregate. The Mg# and Al content in our samples are similar to those described by Rehfeldt et al. (2007), while Na content is significantly lower (Fig. 3B). Small grains of orthopyroxene enclosed in clinopyroxene III have Mg#= 90.8-91.9. Olivine III in the intergranular aggregates has Fo=88.6- 91.7, while NiO and Ca are 0.24-0.34 wt.% and 370-2240 ppm, respectively (Fig. 3C, Table S2). The Fo content in olivine I and III does not change significantly, while NiO and CaO contents are elevated in olivine III; exceptions are the olivine III grains occurring at the outer margins of the biggest aggregates which do not show elevated Ca contents. The glass has a composition of trachyte or trachydacite and dacite (Fig. 4; SiO_2= 63.75-68.35 wt. %; Na_2O+K_2O=4.73-8.84 wt.%; Table S3).

The chemical composition of the altered, hydrous, high Mg glass-like phase is very heterogeneous; Al_2O_3 content varies from 10.7 to 20.4 wt.% and MgO is between 14.7 and 20.7 wt.% (Table S3).

5.2. Chemical composition of phases forming spongy rims and grains

Spongy clinopyroxene III has Mg# from 90.4 to 93.6 (Fig. 3A; Table S1). The Al and Na contents are 0.066-0.271 and 0.024-0.083 apfu, respectively (Fig. 3A,B; Table S1). When compared to clinopyroxene I, spongy clinopyroxene is usually (but not in all cases) lower in Al and Fe (Fig. 3A). The spongy spinel formed of vermicular crystals has a homogenous composition of Cr# = 29.4-32.7 and Mg#=64.2-77.0 (Fig. 3D; Table S4); those values are higher and lower, respectively, than in spinel I in the same sample.

6. Discussion

6.1. Origin of intergranular fine-grained aggregates

Intergranular aggregates in peridotites from Scania were discussed by Rehfeldt et al. (2007; their “resorbed patches”), who suggested that they were remnants of the breakdown of metasomatic amphibole. However, in the set of xenoliths examined in this study, no hydrous phase (e.g. amphibole) was detected and no textures or minerals characteristic for amphibole decomposition (Shaw, 2009) were stated. Therefore, we claim that the studied intergranular aggregates are not a product of amphibole decomposition.

Glass occurring within the aggregates has trachytic/trachydacitic and dacitic (63.8-68.4 wt.% of SiO_2) composition that differs significantly from the host basanite (42.0-44.5 wt.% of SiO_2; Tappe et al., 2016; Fig. 4) composition precluding the possibility of being a product of its infiltration. Aggregates are typically associated with orthopyroxene I grains and formed along their margins. Only within the thickest aggregates, orthopyroxene I is not present suggesting that the formation of the aggregates may be related to its decomposition. Decomposition of orthopyroxene to olivine, clinopyroxene, and Si-rich glass requires the presence of a Si-undersaturated melt that would trigger the reaction (“solvent” in Shaw & Dingwell, 2008; Shaw et al., 2006). Experimental studies by Shaw and Dingwell (2008) showed that during this reaction a Si-rich melt, similar in composition to the Scania glass,

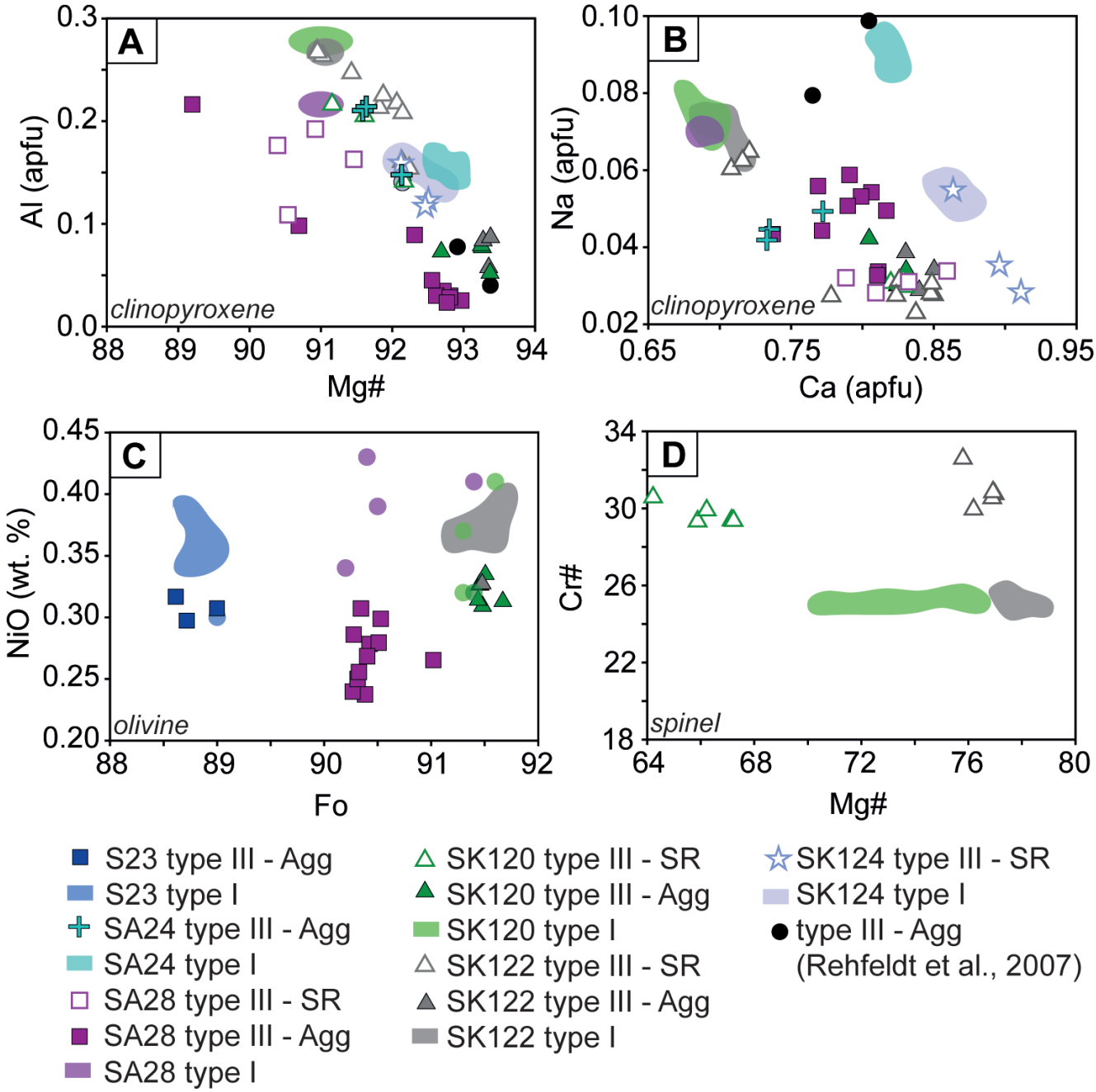

Figure 3. The chemical composition of minerals: (A) Mg# vs. Al content in clinopyroxene III and clinopyroxene I; (B) Ca vs. Na content in clinopyroxene III and I; (C) Fo vs. NiO content in olivine III compared to olivine I; (D) Mg# vs. Cr# in spinel III compared to spinel I. Fields for type I minerals are given for comparison with a chemical composition of spongy (type III – SR) and aggregate-forming type III (type III – Agg) minerals (unpublished data by Mikrut et al.). Data presented in the figure are representative for clarity reasons; the full data set is given in the Supplementary Materials.

is produced. Furthermore, Kelemen (1990) pointed that during the reaction of peridotite with tholeiitic basalt orthopyroxene dissolves while olivine crystallizes, under nearly isenthalpic conditions. Interaction of such melts with ultramafic wall rock often produces calc-alkaline, Si-rich derivative liquids. Compositions of both experimental and theoretical melts fit well to the composition of glasses in Scania peridotites suggesting that they are products of orthopyroxene dissolution. However, in Scania, remnants of the Si-undersaturated melt were not recorded, suggesting that the ratio between orthopyroxene and infiltrating Si-undersaturated melt was <1 and the whole volume of the melt reacted.

The texture and modal composition of the phases participating in the studied intergranular aggregates vary with their thickness (see section 5.1 and Fig. 2C-E). The narrowest aggregates, which envelop the margins of orthopyroxene I consist of clinopyroxene III, olivine III and remnants of orthopyroxene I and represent a product of orthopyroxene decomposition. Textural position and similarities in chemical composition between orthopyroxene enclosed in the fine-grained aggregates and orthopyroxene I (Mg# = 89.4-91.9, Al = 0.106-0.220 apfu; Mikrut et al., 2019) suggest that they constitute the remnants of unreacted orthopyroxene I grain at the initial stage of orthopyroxene I breakdown. Larger aggregates represent a more developed stage

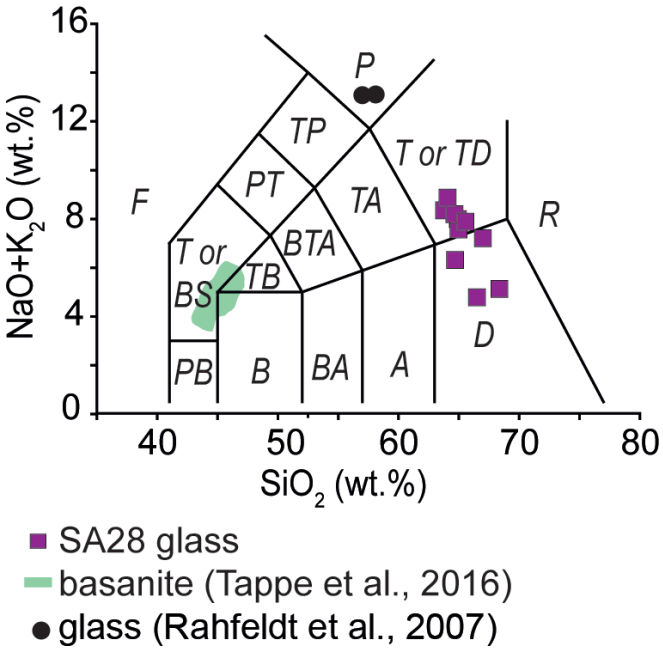

Figure 4. The Total Alkali Silica diagram (after Le Maitre et al., 1989) showing the chemical composition of glass from Scania peridotitic xenoliths from this study in comparison to glass studied by Rehfeldt et al. (2007) and host basanite from Scania (Tappe et al., 2016).

of the reaction between Si-undersaturated melt and orthopyroxene. The increase in size and the development of the intergranular structures suggest a prolonged reaction time which ultimately resulted in the complete decomposition of orthopyroxene (Fig. 2E). This interpretation is in agreement with the location of specific types of aggregates – orthopyroxene-free aggregates are predominantly located near the xenolith margins. More than 1 cm away from the contact with the basanite, the aggregates become narrower, but remnants of orthopyroxene I are present. In the central parts of the xenolith (>2.5 cm from contact), the aggregates, which envelop orthopyroxene I grains, are the narrowest and limited to single crystals of olivine III, clinopyroxene III, and remnants of orthopyroxene I grains.

In the thickest, most developed aggregates the outer parts of the aggregates are formed only of olivine III (Fig. 2E). As discussed, the modal composition of the inner part is a result of orthopyroxene I dissolution. Olivine occurring in the outer zones of the aggregates could have been formed in the same process, but it does not show enrichment in Ca, characteristic for olivine III in the aggregates. The formation of those olivine III may result from partial, dissolution of olivine I due to a reaction with Si-undersaturated melt (Shaw & Dingwell, 2008). The lack of Ca enrichment in olivine III suggests an isothermal process (Brey et al., 1990).

6.2. Origin of the spongy domains

Spongy rims are common in xenolithic peridotites (Lu et al., 2015; Pan et al., 2018). Hirose and Kawamoto (1995) and Shaw et al. (2006) described sieve-textured clinopyroxene characterized by a decrease in Na, Al and an increase in Ca content and aligned with the compositional changes induced during the earliest stages of partial melting. Shaw et al. (2006) interpreted the development of the sieve texture as a result of selective removal of more fusible components, leaving a refractory residue. Sieve-textured clinopyroxene and spinel form in the presence of a Si-rich melt, which migrates along grain boundaries and interacts with spinel and clinopyroxene.

The spongy clinopyroxene III form Scania has lower Al_2O_3 and Na_2O but higher CaO and Mg# than the primary clinopyroxene I (Fig. 3A,B) and the spongy spinel III exhibit depletion in Mg and Al content compared to spinel I. Therefore, the spongy domains in Scania peridotites could have been formed due to a reaction with Si-rich melt as described by Shaw et al. (2006).

6.3. Evolutional relationships between fine-grained aggregates and spongy domains

Fine-grained aggregates and spongy domains are found within the same Scania peridotite xenoliths. Similar structures have been documented worldwide (e.g. in xenoliths from Sal Island; Shaw et al., 2006). Based on petrological observations and geochemical composition, we suggest a mechanism for forming fine-grained aggregates and spongy domains in peridotites from Scania similar to that in xenoliths from Sal Island (Shaw et al., 2006). In this model, the formation of fine-grained aggregates involves the reaction of orthopyroxene with a Si-undersaturated melt, resulting in the production of aggregates composed of olivine, clinopyroxene, and a Si-rich melt. The varying thickness of fine-grained zones, as well as completely reacted grains, indicate differences in the duration of the reaction. The Si-rich melt derived from the breakdown of orthopyroxene migrated along grain boundaries, where it interacted with spinel and clinopyroxene grains, leading to the formation of spongy rims.

The occurrence of a hydrous, high-Mg glass-like phase is associated with fine-grained aggregates. The quantity of this phase varies depending on the width of the fine-grained aggregate zones. The highest concentrations of the hydrous, high-Mg glass-like phase are observed in areas where the fine-grained aggregate zones are the widest or between adjacent fine-grained aggregates. This glass-like phase is highly heterogeneous, with significant variations in Mg and Al content. It is not possible to introduce so high-Mg melt in mantle conditions, so we assume that the process of high Mg glass-like phase formation operated inside the xenolith. We suggest that the hydrous, high-Mg glass-like phase may represent products of *in-situ* melting of the fine-grained aggregates. The aggregates are formed of unevenly distributed olivine and clinopyroxene grains therefore their melting could result in a Mg-rich melt/mixture with a highly heterogeneous chemical composition. We propose that the local reheating and melting of the fine-grained aggregates could take during

their ascent to the surface, under conditions close to the solidus.

7. Conclusions

The xenoliths from Scania do not record typical host volcanic melt infiltration with the introduction of new phases (e.g. plagioclase, magmatic pyroxenes and olivine, sulfides, oxides), but were limited to Si-undersaturated melt that triggered the decomposition of orthopyroxene, which in turn produced Si-rich melt. The effects of the reactions between the melts and minerals differed in specific parts of xenoliths, probably due to the duration of the reaction – in the outermost parts, the reactions were intensive and whole grains of orthopyroxene were dissolved, while spinel and clinopyroxene were enveloped by spongy rims.

As the stage of the development of the aggregates is related with its position within the xenoliths they must have been formed either during the xenoliths formation or immediately after xenoliths extraction from the mantle. In any case, it did not constitute a part of evolution of the lithospheric mantle in this area. This finding simplifies the reconstruction of the evolution of mantle beneath the south-west margin of the East European Craton.

Acknowledgments

Mateusz Ćwiek is thanked for his assistance with fieldwork and Wiktoria Gmochowska is thanked for her help with the glass analyses in Cracow. We are grateful to Levente Patkó for his detailed and insightful review. This study was possible thanks to the project no. NCN UMO-2016/23/B/ST10/01905 (National Science Centre) for MM-M, and to the bilateral Austrian-Polish projects (WTZ PL 08/2018, WTZ PL16).

Competing Interests

The authors declare no competing interests.

Supplementary Data

Supplementary data to this article can be found online at https://doi.org/10.2478/mipo-2025-0002.

References

Artemieva, I. M. (2003). Lithospheric structure, composition, and thermal regime of the East European Craton: Implications for the subsidence of the Russian platform. *Earth and Planetary Science Letters, 213*(3–4), 431–446. https://doi.org/10.1016/S0012-821X(03)00327-3

Asch, K. (2005). *IGME 5000: 1 : 5 Million International Geological Map of Europe and Adjacent Areas - final version for the internet*. BGR, Hannover.

Babuška, V., & Plomerová, J. (2004). The Sorgenfrei–Tornquist Zone as the mantle edge of Baltica lithosphere: new evidence from three-dimensional seismic anisotropy. *Terra Nova*, *16*(5), 243–249. https://doi.org/10.1111/j.1365-3121.2004.00558.x

Bergelin, I., Obst, K., Söderlund, U., Larsson, K., & Johansson, L. (2011). Mesozoic rift magmatism in the North Sea region: 40Ar/39Ar geochronology of Scanian basalts and geochemical constraints. *International Journal of Earth Sciences*, *100*(4), 787–804. https://doi.org/10.1007/s00531-010-0516-3

Bingen, B., Viola, G., Möller, C., Vander Auwera, J., Laurent, A., & Yi, K. (2021). The Sveconorwegian orogeny. *Gondwana Research*, *90*, 273–313. https://doi.org/10.1016/j.gr.2020.10.014

Brey, G. P., Köhler, T., & Nickel, K. G. (1990). Geothermobarometry in Four-phase Lherzolites I. Experimental Results from 10 to 60kb. *Journal of Petrology, 31*(6), 1313–1352. https://doi.org/10.1093/petrology/31.6.1313

Carpenter, R. L., Edgar, A. D., & Thibault, Y. (2002). Origin of spongy textures in clinopyroxene and spinel from mantle xenoliths, Hessian Depression, Germany. *Mineralogy and Petrology*, *74*(2), 149–162. https://doi.org/10.1007/s007100200002

Coltorti, M., Bonadiman, C., Hinton, R. W., Siena, F., & Upton, B. G. J. (1999). Carbonatite Metasomatism of the Oceanic Upper Mantle: Evidence from Clinopyroxenes and Glasses in Ultramafic Xenoliths of Grande Comore, Indian Ocean. *Journal of Petrology*, *40*(1), 133–165. https://doi.org/10.1093/petroj/40.1.133

Deer, W. A., Howie, R. A., & Zussman, J. (1993). *An Introduction to the Rock-Forming Minerals*. Longman Scientific & Technical.

Demouchy, S., Jacobsen, S., Gaillard, F., & Stern, C. (2006). Rapid magma ascent recorded by water diffusion profiles in mantle olivine. *Geology*, *34*, 429–432. https://doi.org/10.1130/G22386.1

Erlström, M. (2009). Tectonic evolution and geological framework of Scania. A review of interpretations and geological models. *SGU-report 2009*:10

Falus, G., Szabó, C., & Vaselli, O. (2000). Mantle upwelling within the Pannonian Basin: evidence from xenolith lithology and mineral chemistry. *Terra Nova*, *12*(6), 295–302. https://doi.org/10.1046/j.1365-3121.2000.00313.x

Geological Survey of Sweden Digital Database. (2018) Https://Www.Sgu.Se/En/Products/Geological-Data/.

Hirose, K., & Kawamoto, T. (1995). Hydrous partial melting of lherzolite at 1 GPa: The effect of H_2O on the genesis of basaltic magmas. *Earth and Planetary Science Letters*, *133*(3), 463–473. https://doi.org/10.1016/0012-821X(95)00096-U

Ionov, D. A., Hofmann, A. W., & Shimizu, N. (1994). Metasomatism-induced Melting in Mantle Xenoliths from Mongolia. *Journal of Petrology, 35*(3), 753–785. https://doi.org/10.1093/petrology/35.3.753

Johansson, Å., Bogdanova, S., & Čečys, A. (2006). A revised geochronology for the Blekinge Province, southern Sweden. *GFF*, *128*(4), 287–302. https://doi.org/10.1080/11035890601284287

Kelemen, P. B. (1990). Reaction Between Ultramafic Rock and Fractionating Basaltic Magma I. Phase Relations, the Origin of Calc-alkaline Magma Series, and the Formation of Discordant Dunite. *Journal of*

Petrology, *31*(1), 51–98. https://doi.org/10.1093/petrology/31.1.51

Le Maitre, R. W., Bateman, P., Dudek, A., Keller, J., Lameyre Le Bas, M. J., Sabine, P. A., Schmid, R., Sorensen, H., Streckeisen, A., Woolley, A. R., & Zanettin, B. (1989). *A Classification of Igneous Rocks and Glossary of Terms* (p. 193). Blackwell.

Lu, J., Zheng, J., Griffin, W. L., O'Reilly, S. Y., & Pearson, N. J. (2015). Microscale effects of melt infiltration into the lithospheric mantle: Peridotite xenoliths from Xilong, South China. *Lithos*, *232*, 111–123. https://doi.org/10.1016/j.lithos.2015.06.013

Marchev, P., Arai, S., Vaselli, O., Costa, F., Zanetti, A., & Downes, H. (2017). Metasomatic Reaction Phenomena from Entrainment to Surface Cooling: Evidence from Mantle Peridotite Xenoliths from Bulgaria. *Journal of Petrology*, *58*(3), 599–640. https://doi.org/10.1093/petrology/egx028

Matusiak-Malek, M., Puziewicz, J., Ntaflos, T., Grégoire, M., Benoit, M., & Klügel, A. (2014). Two contrasting lithologies in off-rift subcontinental lithospheric mantle beneath central Europec-the Krzeniów (SW Poland) case study. *Journal of Petrology*, *55*(9), 1799–1828. https://doi.org/10.1093/petrology/egu042

Mikrut, J., Matusiak-Małek, M., Puziewicz, J., Ntaflos, T., Grégoire, M., Benoit, M., & Johansson, L. (2019). Heterogeneous mantle beneath S Sweden-evidences from peridotitic xenoliths. In *Geophysical Research Abstracts* 21, EGU2019-15595

Pan, S., Zheng, J., Yin, Z., Griffin, W. L., Xia, M., Lin, A., & Zhang, H. (2018). Spongy texture in mantle clinopyroxene records decompression-induced melting. *Lithos*, *320–321*, 144–154. https://doi.org/10.1016/j.lithos.2018.08.035

Rehfeldt, T., Obst, K., & Johansson, L. (2007). Petrogenesis of ultramafic and mafic xenoliths from Mesozoic basanites in southern Sweden: Constraints from mineral chemistry. *International Journal of Earth Sciences*, *96*(3), 433–450. https://doi.org/10.1007/s00531-006-0116-4

Shaw, C. S. J. (2009). Textural development of amphibole during breakdown reactions in a synthetic peridotite. *Lithos*, *110*(1), 215–228. https://doi.org/10.1016/j.lithos.2009.01.002

Shaw, C. S. J., & Dingwell, D. B. (2008). Experimental peridotite–melt reaction at one atmosphere: a textural and chemical study. *Contributions to Mineralogy and Petrology*, *155*(2), 199–214. https://doi.org/10.1007/s00410-007-0237-1

Shaw, C. S. J., Heidelbach, F., & Dingwell, D. B. (2006). The origin of reaction textures in mantle peridotite xenoliths from Sal Island, Cape Verde: the case for "metasomatism" by the host lava. *Contributions to Mineralogy and Petrology*, *151*(6), 681–697. https://doi.org/10.1007/s00410-006-0087-2

Shaw, C. S. J., & Klügel, A. (2002). The pressure and temperature conditions and timing of glass formation in mantle-derived xenoliths from Baarley, West Eifel, Germany: the case for amphibole breakdown, lava infiltration and mineral – melt reaction. *Mineralogy and Petrology*, *74*(2), 163–187. https://doi.org/10.1007/s007100200003

Su, B. X., Zhang, H. F., Sakyi, P. A., Yang, Y. H., Ying, J. F., Tang, Y. J., Qin, K. Z., Xiao, Y., Zhao, X. M., Mao, Q., & Ma, Y. G. (2011). The origin of spongy texture in minerals of mantle xenoliths from the Western Qinling, central China. *Contributions to Mineralogy and Petrology*, *161*(3), 465–482. https://doi.org/10.1007/s00410-010-0543-x

Tappe, S. (2004). Mesozoic mafic alkaline magmatism of southern Scandinavia. *Contributions to Mineralogy and Petrology*, *148*(3), 312–334. https://doi.org/10.1007/s00410-004-0606-y

Tappe, S., Smart, K. A., Stracke, A., Romer, R. L., Prelević, D., & van den Bogaard, P. (2016). Melt evolution beneath a rifted craton edge: 40Ar/39Ar geochronology and Sr–Nd–Hf–Pb isotope systematics of primitive alkaline basalts and lamprophyres from the SW Baltic Shield. *Geochimica et Cosmochimica Acta*, *173*, 1–36. https://doi.org/10.1016/j.gca.2015.10.006

Received: 10 Nov 2024
Accepted: 08 Jan 2025
Handling Editor: Abigail Barker